HHS Public Access

Author manuscript

Ann Biomed Eng. Author manuscript; available in PMC 2018 April 01.

Published in final edited form as:

Ann Biomed Eng. 2017 April ; 45(4): 939–948. doi:10.1007/s10439-016-1753-9.

High Resolution Ultrasound Superharmonic Perfusion Imaging: *In Vivo* Feasibility and Quantification of Dynamic Contrast-Enhanced Acoustic Angiography

Brooks D. Lindsey[1], **Sarah E. Shelton**[1], **K. Heath Martin**[1], **Kathryn A. Ozgun**[1], **Juan D. Rojas**[1], **F. Stuart Foster**[2], and **Paul A. Dayton**[1,3]

[1]Joint Department of Biomedical Engineering, University of North Carolina at Chapel Hill and North Carolina State University, Raleigh, NC, USA

[2]Sunnybrook Health Sciences Centre, Toronto, ON, Canada

[3]Biomedical Research Imaging Center, University of North Carolina at Chapel Hill, Chapel Hill, NC, USA

Abstract

Mapping blood perfusion quantitatively allows localization of abnormal physiology and can improve understanding of disease progression. Dynamic contrast-enhanced ultrasound is a low-cost, real-time technique for imaging perfusion dynamics with microbubble contrast agents. Previously, we have demonstrated another contrast agent-specific ultrasound imaging technique, acoustic angiography, which forms static anatomical images of the superharmonic signal produced by microbubbles. In this work, we seek to determine whether acoustic angiography can be utilized for high resolution perfusion imaging *in vivo* by examining the effect of acquisition rate on superharmonic imaging at low flow rates and demonstrating the feasibility of dynamic contrast-enhanced superharmonic perfusion imaging for the first time. Results in the chorioallantoic membrane model indicate that frame rate and frame averaging do not affect the measured diameter of individual vessels observed, but that frame rate does influence the detection of vessels near and below the resolution limit. The highest number of resolvable vessels was observed at an intermediate frame rate of 3 Hz using a mechanically-steered prototype transducer. We also demonstrate the feasibility of quantitatively mapping perfusion rate in 2D in a mouse model with spatial resolution of ~100 μm. This type of imaging could provide non-invasive, high resolution quantification of microvascular function at penetration depths of several centimeters.

Keywords

Ultrasound; Perfusion; Microbubble; High frequency; Low flow imaging; Quantitative imaging; Angiogenesis; Superharmonic

Address correspondence to Paul A. Dayton, Biomedical Research Imaging Center, University of North Carolina at Chapel Hill, Chapel Hill, NC, USA. padayton@email.unc.edu.

CONFLICT OF INTEREST

The authors declare that they have no conflict of interests with any other companies listed in this paper.

INTRODUCTION

By combining quantitative measurements of physiology with the anatomical localization in traditional medical imaging, high resolution quantitative imaging may both increase diagnostic confidence and improve our understanding of disease processes. The ability to quantitatively map blood perfusion using existing techniques already provides great value in clinical settings, as mapping local hemodynamics lends insight into progression of cancers of the liver,[23, 70] kidney,[53] and pancreas[26, 29] as well as cardiovascular[25, 62] and cerebrovascular disease,[9, 67] and obstetrics.[1, 55] While blood perfusion dynamics are currently quantified *in vivo* using ultrasound, CT, MRI, and nuclear medicine,[10, 20, 49] resolution is currently limited to 200–500 μm for most clinical ultrasound systems,[54] ~600 μm for CT,[53] ~1.6 mm for MRI,[47] and 5–10 mm for SPECT.[20] Alternatively, optical and photoacoustic approaches to vascular imaging have demonstrated spatial resolutions of ~7 and ~50 μm, respectively, but penetration depths are limited to ~1 and ~3 mm respectively.[32, 72]

Ultrasound has been particularly useful as a relatively inexpensive, real-time imaging modality which neither exposes patients to ionizing radiation nor utilizes nephrotoxic contrast agents. Most clinical ultrasound systems are capable of performing 2D perfusion imaging with resolutions of ~500 μm at penetration depths of 5–7 cm,[54] though some preclinical systems achieve higher resolutions.[15] In dynamic contrast-enhanced ultrasound imaging, variations in perfusion are quantified by injecting a bolus of microbubbles and analyzing the time-intensity curve (i.e. “wash-in” or “wash-out”), or by infusing contrast agent, transmitting an ultrasound pulse that is destructive to microbubbles, and measuring the reperfusion characteristics.[10] These perfusion characteristics can be mapped by forming parametric images of the time required to reach a threshold enhancement (e.g., time to peak enhancement or time to 20% of peak) on a per-pixel basis.[26, 30, 61]

Recently, several research groups have demonstrated super-resolution approaches which enable imaging and velocity mapping at resolutions much higher (~20 μm) than typical diffraction-limited ultrasound imaging based on the superposition of microbubbles in many thousands of high-frame rate acquisitions.[7, 12, 35, 51, 66] However, because these techniques seek to localize single bubbles over thousands of sequential acquisitions, they require acquisition and processing of very large amounts of data, and remain very challenging to implement in real-time. Alternatively, other researchers have recently presented new microbubble-based approaches for characterizing microvascular morphology.[31, 43, 46] While microbubbles allow direct tracking of hemodynamics by serving as strong acoustic scatterers within vasculature, Doppler-based techniques for imaging blood flow have been in wide clinical use for decades without the use of exogenous contrast agents.[3, 52] However, the filters utilized in Doppler imaging to remove slow-moving signals from vessel walls also typically eliminate slower velocity blood flow signals. Several techniques for perfusion imaging at slow flow rates without microbubbles have recently been developed.[33, 63] In addition, two commercial manufacturers have recently introduced techniques for high resolution, low flow imaging[16, 64] which are currently under clinical investigation.[8, 71]

Our group has previously demonstrated a high-resolution (~100 *l*m) approach for imaging microvascular structure based on the superharmonic signal produced by microbubbles.[17–19, 58] By transmitting at a lower frequency (<6 MHz) and receiving at much higher frequencies (‡20 MHz), microbubble-generated signals having amplitudes many times higher than tissue signals can be acquired, producing images of microvascular anatomy with high contrast-to-tissue ratios (CTR) of approximately 25 dB.[39, 40] However, this technique is also at least partially destructive to microbubbles,[38] making it challenging to use superharmonic signals from microbubbles to image hemodynamics. In spite of this limitation, we have recently demonstrated the ability to perform molecular imaging of microbubbles bound to endothelial cell markers,[41, 59] suggesting that other techniques which require reception of superharmonic signals arising from repeated pulsing of the same population of microbubbles may also be possible. Extending this superharmonic approach to dynamic perfusion imaging might increase resolution and improve rejection of tissue signals relative to current ultrasound perfusion imaging techniques.

In this article, we seek to determine whether acoustic angiography (superharmonic ultrasound imaging) can be utilized for high resolution perfusion imaging *in vivo*. This is assessed by first examining the effect of acquisition rate on quantitative image-derived measurements in a slow flow environment, the developing chicken embryo. This model allows for assessment of image quality at low perfusion rates and informs the acquisition rate necessary to image various perfusion rates *in vivo*. Secondly, in order to assess feasibility within a broader set of flow scenarios, the application of dynamic superharmonic perfusion imaging is demonstrated in a mouse model.

MATERIALS AND METHODS

Imaging System

In this work, we utilized a prototype dual-frequency transducer consisting of an outer annular element used for transmitting at 4 MHz and a central 30 MHz element for receiving microbubble signals (Fig. 1).[19] This mechanically-steered probe has a fixed axial focus of 12.7 mm and connects to a high-frequency pre-clinical imaging system (VisualSonics Vevo 770, Toronto, ON, Canada) in order to form sector scan images (25.0 mm 9 24.3 mm) at frame rates from 1–10 frames/s. The transducer is mounted on a computer-controlled motion stage which translates the probe in the elevation direction in order to acquire a 3D volume. For all imaging described in this article, the peak negative pressure was 1.2 MPa (MI = 0.6, non-derated).

Varying Acquisition Rate in the Chorioallantoic Membrane Model

The chorioallantoic membrane (CAM) in the developing chicken embryo was used in order to examine the dependence of spatial resolution on frame rate in small vessels (both resolvable and sub-resolution vessels) *in vivo* while comparing with a resolution gold standard, optical microscopy. The chorioallantoic membrane, which allows gas exchange to the developing chicken embryo, has easily accessible superficial networks of fine vasculature. This model has been used in several previous contrast-enhanced ultrasound studies as well as numerous other studies in developmental biology and

angiogenesis.[13, 43, 48, 56, 60] Acquiring images at frame rates which are slower than the local reperfusion rate is expected to allow increased microbubble reperfusion and yield imaging volumes having a greater number of smaller vessels, including sub-resolution vessels. By increasing the acquisition frame rate and using frame averaging, acquired imaging volumes are expected to have higher contrast but only contain vessels which were reperfused between acquisitions, typically larger vessels.

Fertilized chicken eggs (broiler line, Ross 708, North Carolina State Chicken Educational Unit, Raleigh, NC, USA) were refrigerated at 6 °C for 3–7 days prior to incubation. Embryos were incubated *in ovo* at 37.5 °C with 70% relative humidity for 3 days, rotating every 4 h using an automated egg rocker (Model 4200/3200, Farm Innovators, Plymouth, IN, USA). After 3 days of incubation, eggs were cracked and embryos transferred to disposable containers[57] and incubated for 14 days at 37.5 °C, 70% humidity, and 2.0% CO_2 (NAPCO 8000 Series, Thermo Scientific, Waltham, MA, USA). After growing to day 14 (Hamburger and Hamilton stage 39–40[21]), the vitelline vein was cannulated to inject 10^1 microbubbles/mL at 0.167μL/min using a calibrated syringe pump (PHD2000, Harvard Apparatus, Hollis ton, MA, USA). At this stage of development, vessel diameters are expected to range from <10μm to greater than 1 mm for the largest vessels.[37, 45] Lipid-shelled microbubbles used in this work were synthesized in-house using a 9:1 molar ratio of DSPC and DSPE-PEG2000 (Avanti Polar Lipids, Alabaster, AL, USA) as previously described[59] and had a mean diameter of 1.1μm. During imaging, the embryo was held in a custom device to ensure the embryo remained in a single plane and to facilitate coupling of the transducer to the adjacent CAM structure with ultrasound gel. Three-dimensional imaging was performed using the transducer in Fig. 1 with a step size of 100μm and a total extent of 20 mm. In-plane imaging length was 25 mm with a pixel size of 50μm. Three volumes were acquired from each embryo at acquisition rates of 1.5, 3.0, and 4.0 frames/s with 2-frame averaging. After ultrasound imaging, the embryo was viewed and photographed through a microscope (94 magnification, Olympus SZH-ILLK, Tokyo, Japan). A 1.6 mm-diameter ball bearing served as a reference object to determine the scale (Fig. 2b). 12 embryos were imaged using this approach.

Acquired acoustic angiography imaging volumes were segmented from the imaging volumes using centerline extraction via height ridge traversal with manually-defined seed points.[2] Briefly, after manually seeding, a vessel centerline is identified by integrating over a tubular object, then boundaries are determined, providing a vessel radius at each point along the centerline. This approach has been used for a variety of modalities including magnetic resonance angiography, computed tomography, and ultrasound.[2] For each acquisition rate, the following metrics were determined: number of vessels per imaging volume, mean vessel diameter, vessel tortuosity (distance metric[4]), and image intensity.

Perfusion Imaging in the Mouse Model

In order to assess the feasibility of dynamic superharmonic imaging, we acquired a cine loop of images in a single plane in five 12-week-old female C3(1)/Tag mice. These mice typically develop tumors at 16 weeks. Mice are expected to exhibit peak blood flow velocities which are approximately 5x the maximum value in a 15-day-old chicken embryo (up to 250 mm/s

in the mouse carotid compared to 10–50 mm/s in the chicken embryo),[6, 42] and thus within ranges more relevant to those found in human imaging (i.e. from ~1 mm/s up to hundreds of mm/s).[69] Mice were anesthetized with isoflurane and body temperature was maintained using a heated imaging stage. All animal studies were performed in accordance with the Institutional Care and Use Committee at the University of North Carolina-Chapel Hill. A solution of $5x10^9$ microbubbles/mL was delivered at 30μL/min using the same syringe pump described previously. 100 frames were acquired in a single plane during microbubble wash-in, which is the maximum number of frames that can be stored by the imaging system. Following this acquisition, a 3D acoustic angiography volume was acquired using a motion stage to translate the transducer in the elevation direction with a step size of 100m while infusing 5×10^9 microbubbles/mL at 30μ/min for approximately 10 s. The single slice cine was processed offline by mapping the intensity of each pixel over the entire acquisition time, then determining the time required to reach 20% of peak enhancement for each pixel (Matlab, The Mathworks, Natick, MA). These times were then inverted to create maps of perfusion rate in 1/s. Perfusion maps were created for all 5 mice and the relationship between vessel diameter and perfusion rate was examined by measuring the vessel diameter and mean perfusion rate of vessels in ImageJ (NIH, Bethesda, MD).

RESULTS

Varying Acquisition Rate in the Chorioallantoic Membrane Model

In comparing the mean diameters of all vessels measured in optical photographs an acoustic angiography volumes (Fig. 2), acoustic angiography lacks the spatial resolution to resolve the smaller vessels observed optically, as the minimum diameter measured in acoustic angiography volumes was 119 ± 27 μm, relative to 65 ± 11μm optically. While the vessel diameters were very similar in acoustic angiography volumes acquired at different frame rates ($p = 0.39$ between 1.5 and 3 Hz; $p = 0.34$ between 3 and 4 Hz, 2-frame averaging; $p = 0.89$ between 1.5 and 4 Hz, 2-frame averaging), the 3 frames/s acquisitions show higher variance than either of the other two, and the highest mean number of vessels. Alternatively, acquiring at 4 frames/s with 2-frame averaging yields much lower variance. Mean vessel tortuosity (Fig. 3b) is similar across all acquisition rates ($p = 0.26$ between 1.5 and 3 Hz; $p = 0.84$ between 3 and 4 Hz, 2-frame averaging; $p = 0.31$ between 1.5 and 4 Hz, 2-frame averaging). Finally, image intensity (Fig. 3c) is lowest for 4 frames/s, 2 frame-averaged acquisitions, although not all differences are significant ($p = 0.53$ between 1.5 and 3 Hz; $p = 0.0034$ between 3 and 4 Hz, 2-frame averaging; $p = 0.0154$ between 1.5 and 4 Hz, 2-frame averaging). It should be noted that the 3D nature of the ultrasound volumes allows detection of additional vessels in depth which are not differentiable in standard optical images and also enables measurement of vessel tortuosity, an inherently 3D measurement which cannot be made in 2D optical images.

In the 4 frames/s, 2 frame-averaged acquisition, the smallest vessels having slower reperfusion rates have not had sufficient time between transmit events for microbubble reperfusion. This phenomenon is shown in Fig. 4, which displays the maximum intensity projection image of the 1.5 frames/s acquisition alone (a), with a 3 frames/s overlay (b), and with a 4 frames/s, 2 frame-averaged overlay (c). In (b), there are some regions in which the

red 1.5 frames/s acquisition shows through the yellow 3 frames/s acquisition, indicative of the higher vessel density in the 1.5 frames/s acquisition. This effect is even more pronounced when the 4 frames/s, 2 frame-averaged acquisition is overlaid onto the 1.5 frames/s acquisition (c).

Perfusion Imaging in the Mouse Model

2D cines consisting of 100 frames were acquired in $n = 5$ mice, immediately followed by acquisition of a 3D acoustic angiography volume. The 2D dynamic contrast-enhanced perfusion image resulting from the 2D cine was spatially registered to the 3D volume of vascular anatomy. This allows the perfusion map (time to 20% peak enhancement) to be overlaid onto the acoustic angiography volume in order to visualize the relationship between microvascular structure and perfusion in this single slice (Fig. 5). In examining the perfusion map in Fig. 5c, the largest vessels can be seen to qualitatively exhibit the highest reperfusion rates (brightest color), while smaller vessels have slower reperfusion rates (darker colors). The relationship between diameter and perfusion rate for all five mice is shown in Fig. 6. A moderate positive correlation between vessel diameter and mean perfusion rate ($q = 0.57$) was observed using the described imaging technique in the 2D cross-sectional perfusion maps of 5 animals. While arteries and veins have different perfusion rates and are not separated in this work, this correlation is significant at a level of $a = 0.05$ ($p = 5.6196\times10^{28}$), and is consistent with previous observations.[24, 50]

DISCUSSION

Effect of Varying Frame Rate

The slowest frame rate tested (1.5 frames/s) enables sensitivity to smaller vessels (Fig. 2c), and the smallest of these vessels fall below the imaging resolution of the current system (~100 μm). Therefore, the 1.5 frames/s acquisition contains many sub-resolution vessels which cannot be segmented. The detection of sub-resolution vasculature also decreases contrast of the resolvable vessels (Fig. 3c), and makes segmentation of individual vessels more difficult in the 1.5 frames/s image (Fig. 3a). The higher frame rates resulted in more conspicuous vessels having diameters in the resolvable range and facilitated segmentation of these vessels (Figs. 2, 3). The higher variance in vessel diameter for the 3 frames/s acquisition is likely due to the fact that this rate allows increased reperfusion in smaller vessels relative to the faster frame rate (4 frames/s), while enabling clearer visualization of the 100–200μm vessels than the slowest frame rate. An example of this is further illustrated in Fig. 4.

Acquisition rate does not seem to affect measured tortuosity (Fig. 3b). Similarly, observed differences in image intensity are indicative of the fact that as frame rate or averaging increase, microbubbles have less time to reperfuse, resulting in fewer microbubbles to image and thus lower observed image intensity. Presence of clouds of microbubbles which do not appear to belong to individual vessels indicates sensitivity to microbubbles in sub-resolution vessels. While this ability to detect microbubbles in sub-resolution vessels can be useful in some scenarios,[11] in other situations it may be preferable to use higher frame rates with

averaging in order to form higher contrast images of moderately-sized vessels for efficient image segmentation.

Sources of Variance and Tradeoffs in Superharmonic Contrast Imaging

By imaging the chorioallantoic membrane model, we have demonstrated that variations in frame rate have little effect on the measured vessel diameter (Fig. 2a), although varying frame rate does affect the diameter to which this imaging technique is sensitive (Fig. 3), due to the underlying relationship between vessel diameter and blood velocity. Also, frame averaging reduces sensitivity to the smallest vessels, as the microbubbles in these vessels are destroyed by the initial pulse and have not had time to reperfuse by the arrival of the second pulse (Figs. 3a, 3c).

In imaging in the mouse model, which has higher reperfusion rates but also higher attenuation than the CAM, we were able to demonstrate the ability to acquire high-resolution parametric perfusion images in a single slice with sensitivity to a range of perfusion rates (Fig. 5). There is future potential for extending other dynamic contrast-enhanced approaches to superharmonic imaging, however they would also be constrained to 2D imaging using this transducer. A dual-frequency array[27, 34, 44, 65] would enable a greater variety of destruction reperfusion techniques by enabling increased spatial control over microbubble destruction as well as increased temporal control over frame rates, an important consideration given that reperfusion rates clearly vary among vessels. It should also be noted that although imaging experiments presented in this article were performed in CAM and mouse models, we have previously demonstrated extensive imaging in rats with penetration depths in the range of 2–3 cm,[17, 59] depths to which the presented perfusion imaging approach is directly applicable. Further extension of the penetration depth would require designing transducers with deeper focal depths and/or lower combinations of frequencies.[28, 34, 40]

Acoustic angiography is a tool for both pre-clinical imaging of animal models and clinical imaging in humans, for which a trial is currently underway. In addition to imaging microvascular anatomy, the creation of high resolution functional imaging techniques—including molecular imaging[41, 59] and perfusion imaging, demonstrated in this article—enables non-invasive physiological mapping in animal models. Further development of dual-frequency transducers in new form factors is required to deliver acoustic angiography to new applications in human imaging.[28, 34, 36]

Dynamic Superharmonic Perfusion Imaging

In this article, we have demonstrated the feasibility of single-slice dynamic contrast-enhanced perfusion imaging using superharmonic signals from microbubbles. The presented approach utilized “time-to-peak” processing on a per-pixel basis, although other approaches such as time-intensity curve analysis could also be utilized with the same superharmonic signals.[10, 22] While the high resolution of these 2D perfusion images suggests potential applications in oncology or cardiology, the ability to acquire 3D perfusion volumes with similarly high resolution and contrast-to-tissue ratio would build on existing 3D perfusion

techniques and could prove to be a powerful clinical tool for localizing abnormalities in blood flow dynamics.[5, 14, 68]

Summary

We have examined the dependence of high resolution acoustic angiography imaging and image-derived measurements on acquisition rate in a low flow scenario in vivo. Results indicate that more microvessels can be identified at a frame rate of 3 Hz, but that the vessels tortuosity as quantified by the distance metric remains similar across frame rates. Increasing frame rate and frame averaging produces images with higher contrast but reduces sensitivity to smaller vessels. We have also developed an approach for high resolution perfusion imaging and have demonstrated its feasibility in five mice, presenting the first dynamic contrast-enhanced superharmonic perfusion image. Development of dual-frequency array transducers may improve the ability to perform dynamic contrast-enhanced perfusion imaging by enabling greater spatial control of transmitted beam profiles and a wider variety of acquisition rates, which may prove useful across various physiological flow environments.

Acknowledgments

This work was supported by Grants R01CA170665, R01CA189479, F32EB018715, and T32HL069768 from the National Institutes of Health. We thank Mike Lee, Jay Son, Emmanuel Cherin, Guofeng Pang, and Chris Chaggares for their contributions to the design and fabrication of prototype transducers. Mouse studies were performed within the Lineberger Comprehensive Cancer Center (LCCC) Animal Studies Core Facility at the University of North Carolina at Chapel Hill. The LCCC Animal Studies Core is supported in part by an NCI Center Core Support Grant (CA16086) to the UNC Lineberger Comprehensive Cancer Center.

F. Stuart Foster is a consultant and receives research funding from VisualSonics, Inc. F. Stuart Foster and Paul A. Dayton are inventors on a pending patent describing the acoustic angiography technology. Paul A. Dayton is a co-founder of SonoVol, Inc., a company which has licensed this patent enabling acoustic angiography.

References

1. Arthuis CJ, Novell A, Escoffre JM, Patat F, Bouakaz A, Perrotin F. New insights into uteroplacental perfusion: quantitative analysis using Doppler and contrast-enhanced ultrasound imaging. Placenta. 2013; 34:424–431. [PubMed: 23518453]
2. Aylward SR, Bullitt E. Initialization, noise, singularities, and scale in height ridge traversal for tubular object centerline extraction. IEEE Trans. Med. Imaging. 2002; 21:61–75. [PubMed: 11929106]
3. Berger M, Haimowitz A, Vantosh A, Berdoff RL, Goldberg E. Quantitative assessment of pulmonary-hypertension in patients with tricuspid regurgitation using continuous wave Doppler ultrasound. J. Am. Coll. Cardiol. 1985; 6:359–365. [PubMed: 4019921]
4. Bullitt E, Gerig G, Pizer SM, Lin W, Aylward SR. Measuring tortuosity of the intracerebral vasculature from MRA images. IEEE Trans. Med. Imaging. 2003; 22:1163–1171. [PubMed: 12956271]
5. Chen NG, Fowlkes JB, Carson PL, Schipper MJ, LeCarpentier GL. Rapid 3-D imaging of contrast flow: application in a perfused kidney phantom. Ultrasound Med. Biol. 2009; 35:813–828. [PubMed: 19345468]
6. Cherin E, Williams R, Needles A, Liu G, White C, Brown AS, et al. Ultrahigh frame rate retrospective ultrasound microimaging and blood flow visualization in mice *in vivo*. Ultrasound Med. Biol. 2006; 32:683–691. [PubMed: 16677928]

7. Christensen-Jeffries K, Browning RJ, Tang MX, Dunsby C, Eckersley RJ. *In vivo* acoustic super-resolution and super-resolved velocity mapping using microbubbles. IEEE Trans. Med. Imaging. 2015; 34:433–440. [PubMed: 25265604]

8. D'Abate F, Ramachandran V, Young MA, Farrah J, Ahmed MH, Jones K, et al. B-flow imaging in lower limb peripheral arterial disease and bypass graft ultra-sonography. Ultrasound Med. Biol. 2016; 42(9):2345–2351. [PubMed: 27222245]

9. Dani KA, Thomas RG, Chappell FM, Shuler K, Muir KW, Wardlaw JM. Systematic review of perfusion imaging with computed tomography and magnetic resonance in acute ischemic stroke: heterogeneity of acquisition and postprocessing parameters: a translational medicine research collaboration multicentre acute stroke imaging study. Stroke. 2012; 43:563–566. [PubMed: 21998057]

10. Dietrich CF, Averkiou MA, Correas JM, Lassau N, Leen E, Piscaglia F. An EFSUMB Introduction into dynamic contrast-enhanced ultrasound (DCE-US) for quantification of tumour perfusion. Ultraschall Der Med. 2012; 33:344–351.

11. Dunleavey JM, Xiao L, Thompson J, Kim MM, Shields JM, Shelton SE, et al. Vascular channels formed by subpopulations of PECAM1 + melanoma cells. Nat. Commun. 2014; 5:5200. [PubMed: 25335460]

12. Errico C, Pierre J, Pezet S, Desailly Y, Lenkei Z, Couture O, et al. Ultrafast ultrasound localization microscopy for deep super-resolution vascular imaging. Nature. 2015; 527:499–502. [PubMed: 26607546]

13. Faez T, Skachkov I, Versluis M, Kooiman K, de Jong N. *In vivo* characterization of ultrasound contrast agents: microbubble spectroscopy in a chicken embryo. Ultrasound Med. Biol. 2012; 38:1608–1617. [PubMed: 22766113]

14. Feingold S, Gessner R, Guracar IM, Dayton PA. Quantitative volumetric perfusion mapping of the microvasculature using contrast ultrasound. Investig. Radiol. 2010; 45:669–674. [PubMed: 20808232]

15. Foster FS, Mehi J, Lukacs M, Hirson D, White C, Chaggares C, et al. A new 15–50 MHz array-based micro-ultrasound scanner for preclinical imaging. Ultrasound Med. Biol. 2009; 35:1700–1708. [PubMed: 19647922]

16. General Electric Corporation. B-flow imaging. Wauwatosa: 2013.

17. Gessner RC, Aylward SR, Dayton PA. Mapping microvasculature with acoustic angiography yields quantifiable differences between healthy and tumor-bearing tissue volumes in a rodent model. Radiology. 2012; 264:733–740. [PubMed: 22771882]

18. Gessner RC, Frederick CB, Foster FS, Dayton PA. Acoustic angiography: a new imaging modality for assessing microvasculature architecture. Int. J. Biomed. Imaging. 2013; 2013:936593. [PubMed: 23997762]

19. Gessner R, Lukacs M, Lee M, Cherin E, Foster FS, Dayton PA. High-resolution, high-contrast ultrasound imaging using a prototype dual-frequency transducer: *in vitro* and *in vivo* studies. IEEE Trans. Ultrason. Ferroelectr. Freq. Control. 2010; 57:1772–1781. [PubMed: 20679006]

20. Greenwood JP, Maredia N, Younger JF, Brown JM, Nixon J, Everett CC, et al. Cardiovascular magnetic resonance and single-photon emission computed tomography for diagnosis of coronary heart disease (CE-MARC): a prospective trial. Lancet. 2012; 379:453–460. [PubMed: 22196944]

21. Hamburger V, Hamilton HL. A series of normal stages in the development of the chick embryo. J. Morphol. 1951; 88:49–92. [PubMed: 24539719]

22. Ignee A, Jedrejczyk M, Schuessler G, Jakubowski W, Dietrich CF. Quantitative contrast enhanced ultrasound of the liver for time intensity curves-Reliability and potential sources of errors. Eur. J. Radiol. 2010; 73:153–158. [PubMed: 19157739]

23. Ippolito D, Sironi S, Pozzi M, Antolini L, Ratti L, Alberzoni C, et al. Hepatocellular carcinoma in cirrhotic liver disease: functional computed tomography with perfusion imaging in the assessment of tumor vascularization. Acad. Radiol. 2008; 15:919–927. [PubMed: 18572129]

24. Jain RK. Determinants of tumor blood flow: a review. Cancer Res. 1988; 48:2641–2658. [PubMed: 3282647]

25. Jogiya R, Kozerke S, Morton G, De Silva K, Redwood S, Perera D, et al. Validation of dynamic 3-dimensional whole heart magnetic resonance myocardial perfusion imaging against fractional flow

reserve for the detection of significant coronary artery disease. J. Am. Coll. Cardiol. 2012; 60:756–765. [PubMed: 22818072]

26. Kersting S, Konopke R, Kersting F, Volk A, Distler M, Bergert H, et al. Quantitative perfusion analysis of trans-abdominal contrast-enhanced ultrasonography of pancreatic masses and carcinomas. Gastroenterology. 2009; 137:1903–1911. [PubMed: 19715694]
27. Kim J, Li SB, Kasoji S, Dayton PA, Jiang XN. Dual-frequency super harmonic imaging piezoelectric transducers for transrectal ultrasound. Health Monit. Struct. Biol. Syst. 2015; 9438:2015.
28. Kim J, Li S, Kasoji S, Dayton PA, Jiang X. Phantom evaluation of stacked-type dual-frequency 1–3 composite transducers: a feasibility study on intracavitary acoustic angiography. Ultrasonics. 2015; 63:7–15. [PubMed: 26112426]
29. Kitano M, Kudo M, Maekawa K, Suetomi Y, Sakamoto H, Fukuta N, et al. Dynamic imaging of pancreatic diseases by contrast enhanced coded phase inversion harmonic ultrasonography. Gut. 2004; 53:854–859. [PubMed: 15138213]
30. Kogan P, Johnson KA, Feingold S, Garrett N, Guracar I, Arendshorst WJ, et al. Validation of dynamic contrast-enhanced ultrasound in rodent kidneys as an absolute quantitative method for measuring blood perfusion. Ultrasound in Med. Biol. 2011; 37:900–908. [PubMed: 21601135]
31. Kuenen MP, Saidov TA, Wijkstra H, Mischi M. Contrast-ultrasound dispersion imaging for prostate cancer localization by improved spatiotemporal similarity analysis. Ultrasound Med. Biol. 2013; 39:1631–1641. [PubMed: 23791350]
32. Leahy C, Radhakrishnan H, Weiner G, Goldberg JL, Srinivasan VJ. Mapping the 3D connectivity of the rat inner retinal vascular network using OCT angiography. Investig. Ophthalmol. Vis. Sci. 2015; 56:5785–5793. [PubMed: 26325417]
33. Li YL, Dahl JJ. Coherent flow power Doppler (CFPD): flow detection using spatial coherence beamforming. IEEE Trans. Ultrason. Ferroelectr. Freq. Control. 2015; 62:1022–1035. [PubMed: 26067037]
34. Li, SB., Kim, J., Wang, ZC., Jiang, XN., Kasoji, S., Lindsey, B., et al. 2015 IEEE International Ultrasonics Symposium (IUS). Taipei: 2015. A 3 MHz/18 MHz dual-layer co-linear array for transrectal acoustic angiography.
35. Lin F, Shelton SE, Espíndola D, Rojas JD, Pinton G, Dayton PA. 3-D ultrasound localization microscopy for identifying microvascular morphology features of tumor angiogenesis at a resolution beyond the diffraction limit of conventional ultrasound. Theranostics. 2017; 7(1):196–204. [PubMed: 28042327]
36. Lindsey, B., Kim, J., Dayton, P., Jiang, X. IEEE International Ultrasonics Symposium, Tours. France: Sep 20. 2016 A dual-frequency endoscopic transducer for imaging vascular invasion in pancreatic cancer.
37. Lindsey BD, Martin KH, Jiang X, Dayton PA. Adaptive windowing in contrast-enhanced intravascular ultrasound imaging. Ultrasonics. 2016; 70:123–135. [PubMed: 27161022]
38. Lindsey BD, Rojas JD, Dayton PA. On the relationship between microbubble fragmentation, deflation, and broadband superharmonic signal production. Ultrasound Med. Biol. 2015; 41:1711–1725. [PubMed: 25766572]
39. Lindsey BD, Rojas JD, Martin KH, Shelton SE, Dayton PA. Acoustic characterization of contrast-to-tissue ratio and axial resolution for dual-frequency contrast-specific acoustic angiography imaging. IEEE Trans. Ultrason. Ferroelectr. Freq. Control. 2014; 61:1668–1687. [PubMed: 25265176]
40. Lindsey BD, Shelton SE, Dayton PA. Optimization of contrast-to-tissue ratio through pulse windowing in dual-frequency “acoustic angiography” imaging. Ultrasound Med. Biol. 2015; 41:1884–1895. [PubMed: 25819467]
41. Lindsey BD, Shelton SE, Foster FS, Dayton PA. Assessment of molecular acoustic angiography for combined microvascular and molecular imaging in preclinical tumor models. Mol. Imaging Biol. 2016; doi: 10.1007/s11307-016-0991-4
42. Ma ZH, Liu AP, Yin X, Troyer A, Thornburg K, Wang RKK, et al. Measurement of absolute blood flow velocity in outflow tract of HH18 chicken embryo based on 4D reconstruction using spectral domain optical coherence tomography. Biomed. Opt. Expr. 2010; 1:798–811.

43. Maresca D, Skachkov I, Renaud G, Jansen K, van Soest G, de Jong N, et al. Imaging microvasculature with contrast-enhanced ultraharmonic ultrasound. Ultrasound Med. Biol. 2014; 40:1318–1328. [PubMed: 24613639]
44. Martin KH, Lindsey BD, Ma J, Lee M, Li S, Foster FS, et al. Dual-frequency piezoelectric transducers for contrast enhanced ultrasound imaging. Sensors (Basel). 2014; 14:20825–20842. [PubMed: 25375755]
45. Martin KH, Lindsey BD, Ma J, Nichols TC, Jiang X, Dayton PA. *Ex vivo* porcine arterial and chorioallantoic membrane acoustic angiography using dual-frequency intravascular ultrasound probes. Ultrasound Med. Biol. 2016; 42:2294–2307. [PubMed: 27260246]
46. Mischi M, Demi L, Smeenge M, Kuenen MP, Postema AW, de la Rosette JJ, et al. Transabdominal contrast-enhanced ultrasound imaging of the prostate. Ultrasound Med. Biol. 2015; 41:1112–1118. [PubMed: 25701535]
47. Motwani M, Maredia N, Fairbairn TA, Kozerke S, Radjenovic A, Greenwood JP, et al. High-resolution versus standard-resolution cardiovascular MR myocardial perfusion imaging for the detection of coronary artery disease. Circ. Cardiovasc. Imaging. 2012; 5:306–313. [PubMed: 22499848]
48. Nowak-Sliwinska P, Segura T, Iruela-Arispe ML. The chicken chorioallantoic membrane model in biology, medicine and bioengineering. Angiogenesis. 2014; 17:779–804. [PubMed: 25138280]
49. O'Connor JP, Tofts PS, Miles KA, Parkes LM, Thompson G, Jackson A. Dynamic contrast-enhanced imaging techniques: CT and MRI. Br. J. Radiol. 2011; 84(2):S112–S120. [PubMed: 22433822]
50. Pries AR, Secomb TW, Gaehtgens P, Gross JF. Blood flow in microvascular networks. Experiments and simulation. Circ. Res. 1990; 67:826–834. [PubMed: 2208609]
51. Provost J, Papadacci C, Demene C, Gennisson JL, Tanter M, Pernot M. 3-D ultrafast doppler imaging applied to the noninvasive mapping of blood vessels *in vivo*. IEEE Trans. Ultrason. Ferroelectr. Freq. Control. 2015; 62:1467–1472. [PubMed: 26276956]
52. Reid JM, Spencer MP. Ultrasonic doppler technique for imaging blood-vessels. Science. 1972; 176:1235–1236. [PubMed: 5033641]
53. Reiner CS, Roessle M, Thiesler T, Eberli D, Klotz E, Frauenfelder T, et al. Computed tomography perfusion imaging of renal cell carcinoma: systematic comparison with histopathological angiogenic and prognostic markers. Investig. Radiol. 2013; 48:183–191. [PubMed: 23328912]
54. Rissanen TT, Korpisalo P, Karvinen H, Liimatainen T, Laidinen S, Grohn OH, et al. High-resolution ultrasound perfusion imaging of therapeutic angiogenesis. JACC Cardiovasc Imaging. 2008; 1:83–91. [PubMed: 19356410]
55. Roberts VH, Lo JO, Salati JA, Lewandowski KS, Lindner JR, Morgan TK, et al. Quantitative assessment of placental perfusion by contrast-enhanced ultrasound in macaques and human subjects. Am. J. Obstet. Gynecol. 2016; 214:369e1–8. [PubMed: 26928151]
56. Schellpfeffer MA, Kolesari GL. Microbubble contrast imaging of the cardiovascular system of the chick embyro. Ultrasound Med. Biol. 2012; 38:504–510. [PubMed: 22266227]
57. Schomann T, Qunneis F, Widera D, Kaltschmidt C, Kaltschmidt B. Improved method for ex ovo-cultivation of developing chicken embryos for human stem cell xenografts. Stem Cells International. 2013; 960958:1–9.
58. Shelton SE, Lee YZ, Foster FS, Lee M, Cherin E, Aylward SR, et al. Quantification of microvascular tortuosity during tumor evolution utilizing acoustic angiography. Ultrasound Med. Biol. 2015; 41:1896–1904. [PubMed: 25858001]
59. Shelton SE, Lindsey BD, Tsuruta JK, Foster FS, Dayton PA. Molecular acoustic angiography: a new technique for high resolution superharmonic ultrasound molecular imaging. Ultrasound Med. Biol. 2016; 42:769–781. [PubMed: 26678155]
60. Stieger SM, Caskey CF, Adamson RH, Qin S, Curry FR, Wisner ER, et al. Enhancement of vascular permeability with low-frequency contrast-enhanced ultrasound in the chorioallantoic membrane model. Radiology. 2007; 243:112–121. [PubMed: 17392250]
61. Streeter JE, Herrera-Loeza SG, Neel NF, Yeh JJ, Dayton PA. A comparative evaluation of ultrasound molecular imaging, perfusion imaging, and volume measurements in evaluating

response to therapy in patient--derived xenografts. Technol. Cancer Res. Treat. 2013; 12:311–321. [PubMed: 23369156]

62. Thomas JD. Myocardial contrast echocardiography perfusion imaging: still waiting after all these years. J. Am. Coll. Cardiol. 2013; 62:1362–1364. [PubMed: 23770171]
63. Tierney, JE., Dumont, DM., Byram, BC. Presented at the SPIE Medical Imaging 2016. San Diego: 2016. “Perfusion” imaging with non-contrast ultrasound.
64. Toshiba Medical Systems Corporation. Seeing the unseen new techniques in vascular imaging: superb micro-vascular imaging. 2014.
65. van Neer PL, Matte G, Danilouchkine MG, Prins C, van den Adel F, de Jong N. Super-harmonic imaging: development of an interleaved phased-array transducer. IEEE Trans. Ultrason. Ferroelectr. Freq. Control. 2010; 57:455–468. [PubMed: 20178912]
66. Viessmann OM, Eckersley RJ, Christensen-Jeffries K, Tang MX, Dunsby C. Acoustic super-resolution with ultrasound and microbubbles. Phys. Med. Biol. 2013; 58:6447–6458. [PubMed: 23999099]
67. Wintermark M, Sesay M, Barbier E, Borbely K, Dillon WP, Eastwood JD, et al. Comparative overview of brain perfusion imaging techniques. J. Neuroradiol. 2005; 32:294–314. [PubMed: 16424829]
68. Xu HX, Lu MD, Xie XH, Xie XY, Xu ZF, Chen LD, et al. Three-dimensional contrast-enhanced ultrasound of the liver: experience of 92 cases. Ultrasonics. 2009; 49:377–385. [PubMed: 19041996]
69. Yang VX, Gordon M, Tang SJ, Marcon N, Gardiner G, Qi B, et al. High speed, wide velocity dynamic range Doppler optical coherence tomography (Part III): *in vivo* endoscopic imaging of blood flow in the rat and human gastrointestinal tracts. Opt. Express. 2003; 11:2416–2424. [PubMed: 19471352]
70. Yang W, Yan K, Wang S, Dai Y, Wu W, Yin SS, et al. Differential diagnosis of arterial phase enhanced hepatic inflammatory lesions and hepatocellular carcinomas with contrast-enhanced ultrasound. Ultrasound Med. Biol. 2016; 42:82–91. [PubMed: 26456578]
71. Zhan J, Diao XH, Jin JM, Chen L, Chen Y. Superb microvascular imaging-a new vascular detecting ultrasonographic technique for avascular breast masses: a preliminary study. Eur. J. Radiol. 2016; 85:915–921. [PubMed: 27130051]
72. Zhang HF, Maslov K, Stoica G, Wang LHV. Functional photoacoustic microscopy for high-resolution and noninvasive *in vivo* imaging. Nat. Biotechnol. 2006; 24:848–851. [PubMed: 16823374]

FIGURE 1.

The prototype dual-frequency transducer used in this work is mechanically steered to acquire in-plane images (red arrow). The entire probe is then translated in the elevation direction using a computer-controlled motion stage to acquire 3D imaging data sets (blue arrow). The central element operates at 30 MHz (receive), and the outer annular element operates at 4 MHz (transmit).

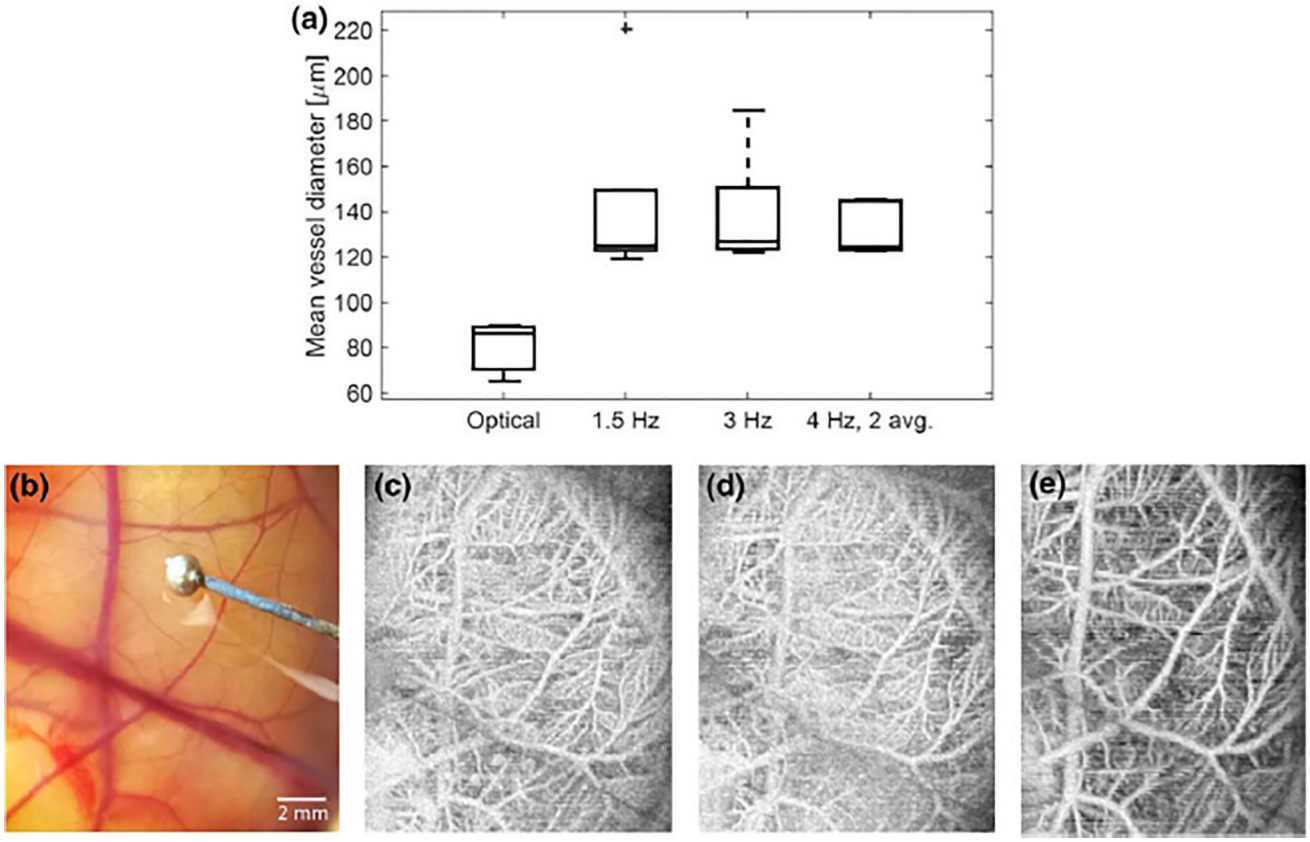

FIGURE 2.

(a) The mean vessel diameter was measured optically and with acoustic angiography in 12 animals, yielding mean values of 65 *l*m (optical) and 119 *l*m (acoustic angiography). (b) Illustrative optical image of the CAM and (c) matched maximum intensity projection in the same embryo at acquisition rates of 1.5, 3, and 4 frames per second (2 frame averaging) show that different vessels are detected with different acquisition rates. The diameter of ball bearing (reference object) in (a) is 1.60 mm.

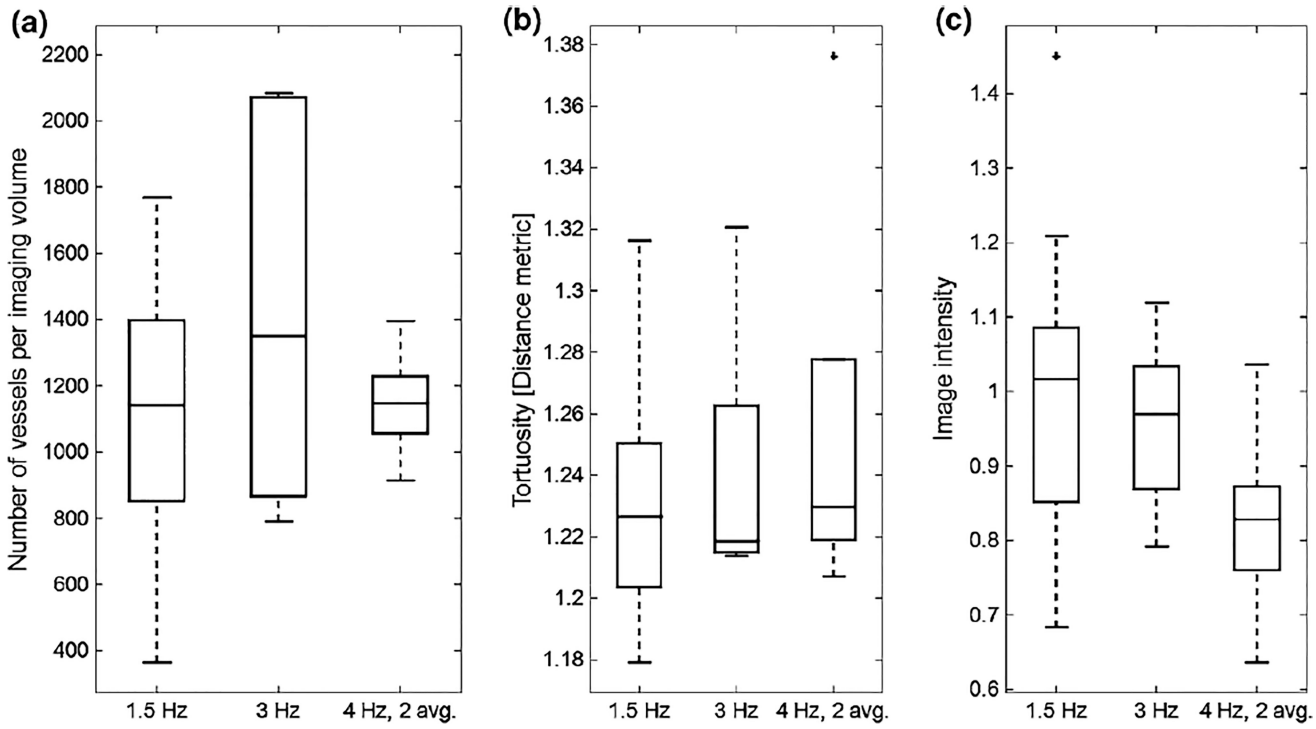

FIGURE 3.

Characteristics measured in the 12 chicken embryos in which images were acquired include (a) number of vessels per imaging volume, (b) tortuosity of those vessels as quantified by the distance metric, and (c) intensity of imaging volumes for three acquisition rates. Although differences were not significant, trends suggest that increasing frame rate does not greatly affect the number of vessels detected in an imaging volume, although acquiring at 4 Hz with 2-frame averaging tends to produce less variation in the number of vessels per volume (a) and lower mean image intensity (c), both which are presumably due to loss of signal from the smallest vessels.

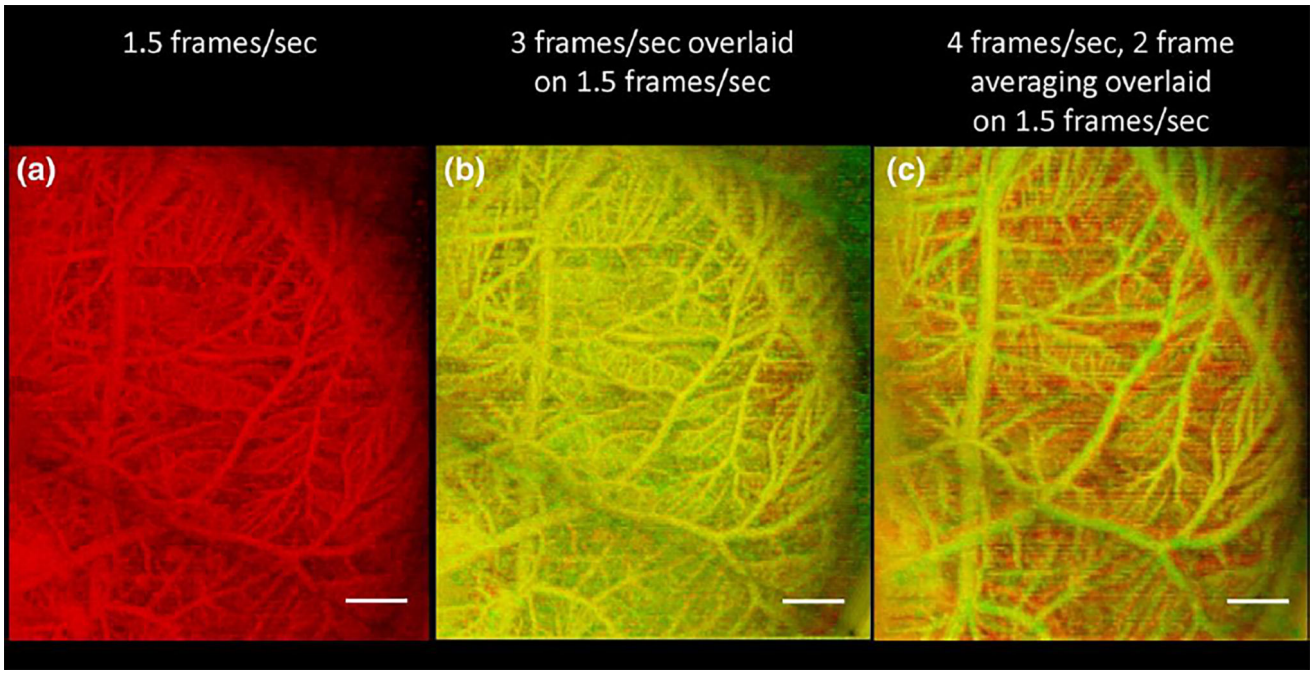

FIGURE 4.

Overlaying images acquired at different rates allows for visualization of resulting differences in which vessels are detected. (a) Maximum intensity projection of chorioallantoic membrane in a chicken embryo acquired at 1.5 frames/s. (b) Overlaid chicken embryo image showing acquisitions at (b) 1.5 frames per second (red) and 3 frames per second (green) indicates isolated locations (shown in red) where the slower frame rate is more sensitive to microbubbles in small vessels, while (c) overlaid acquisitions at 1.5 frames per second (red) and 4 frames per second with 2 frame averaging (green) indicate many locations where the slower frame rate is more sensitive to microbubbles in small vessels. Scale bar indicates 2 mm.

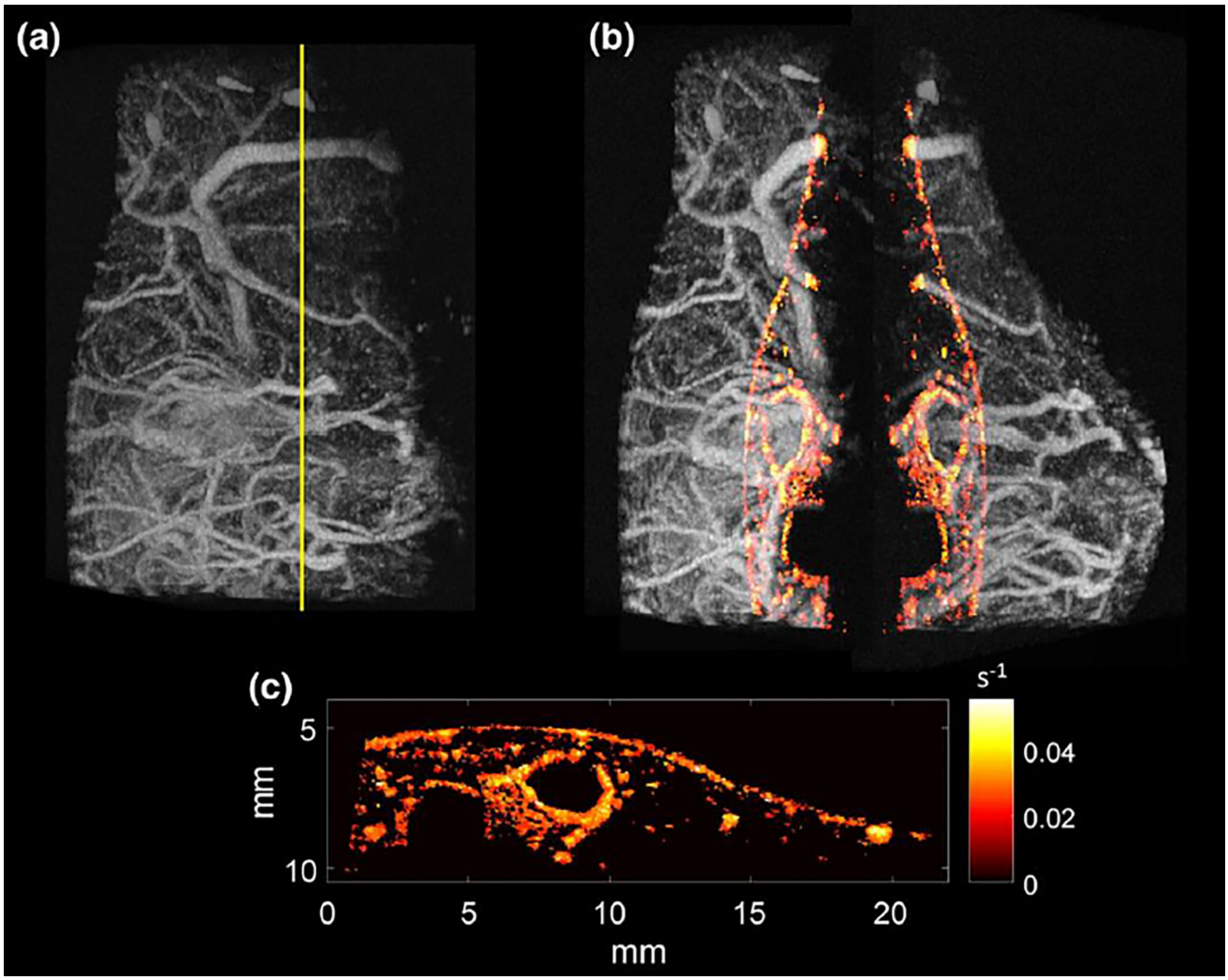

FIGURE 5.

(a) Maximum intensity projection acoustic angiography image acquired in the flank of 12-week-old female C3(1)/Tag mice mouse, with the yellow line indicating the plane in which the perfusion map was acquired. (b) Separated volume with perfusion map overlaid on both sides of volume. (c) Perfusion map alone, with brighter color indicating increased perfusion rate according to the described “time to 20% of peak enhancement” processing.

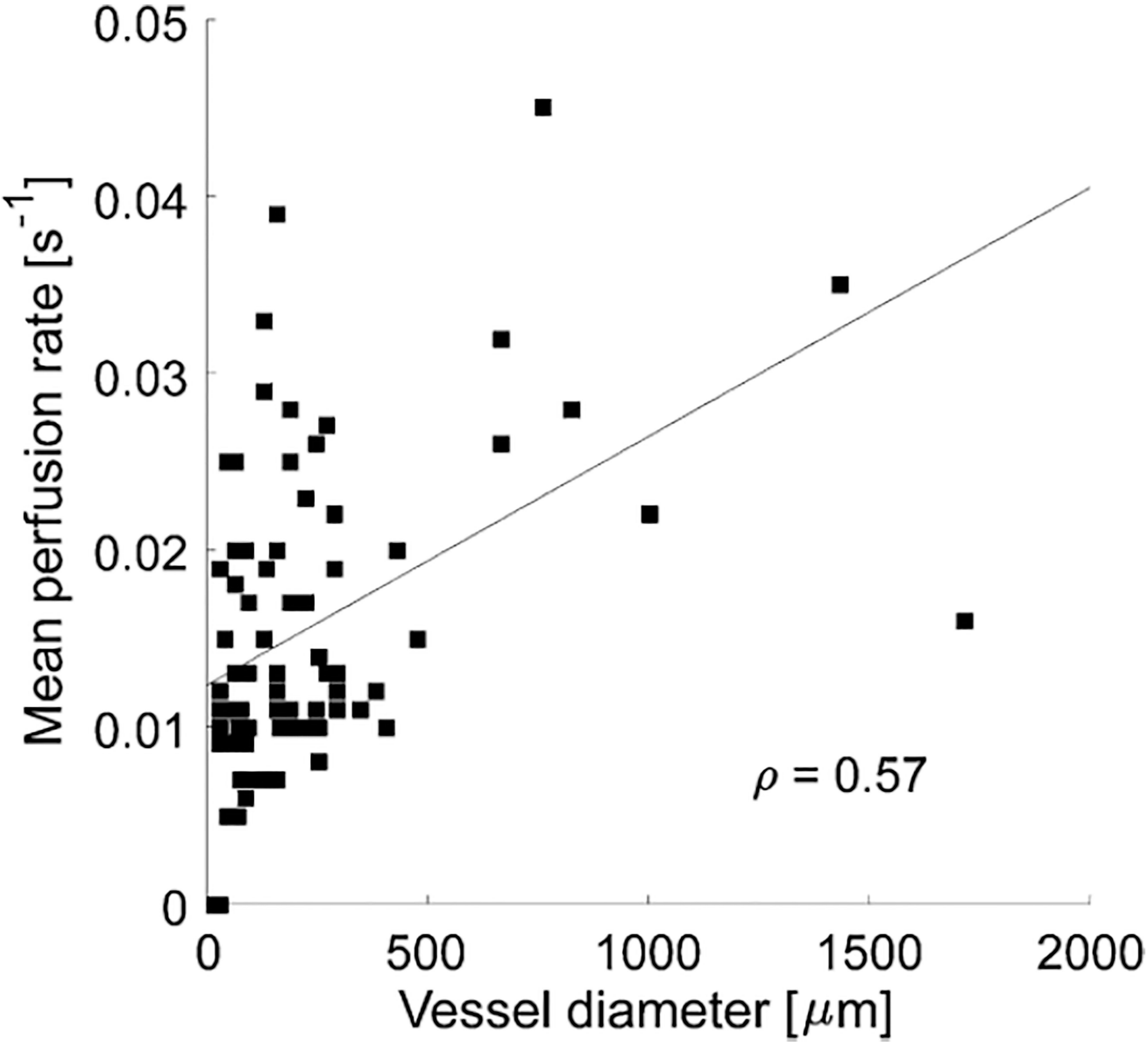

FIGURE 6.

Analyzing the relationship between mean perfusion rate and vessel diameter reveals moderate correlation between mean perfusion rate and vessel diameter for vessels captured in the single-plane perfusion (e.g., Fig. 5c) map in 5 mice (q 5 0.57, p 5 5.6196 3 10^{28}).